NASA/CR—2003-212541

A Simple Model of Pulsed Ejector Thrust Augmentation

Jack Wilson
QSS Group, Inc., Cleveland, Ohio

August 2003

The NASA STI Program Office . . . in Profile

Since its founding, NASA has been dedicated to the advancement of aeronautics and space science. The NASA Scientific and Technical Information (STI) Program Office plays a key part in helping NASA maintain this important role.

The NASA STI Program Office is operated by Langley Research Center, the Lead Center for NASA's scientific and technical information. The NASA STI Program Office provides access to the NASA STI Database, the largest collection of aeronautical and space science STI in the world. The Program Office is also NASA's institutional mechanism for disseminating the results of its research and development activities. These results are published by NASA in the NASA STI Report Series, which includes the following report types:

- TECHNICAL PUBLICATION. Reports of completed research or a major significant phase of research that present the results of NASA programs and include extensive data or theoretical analysis. Includes compilations of significant scientific and technical data and information deemed to be of continuing reference value. NASA's counterpart of peer-reviewed formal professional papers but has less stringent limitations on manuscript length and extent of graphic presentations.

- TECHNICAL MEMORANDUM. Scientific and technical findings that are preliminary or of specialized interest, e.g., quick release reports, working papers, and bibliographies that contain minimal annotation. Does not contain extensive analysis.

- CONTRACTOR REPORT. Scientific and technical findings by NASA-sponsored contractors and grantees.

- CONFERENCE PUBLICATION. Collected papers from scientific and technical conferences, symposia, seminars, or other meetings sponsored or cosponsored by NASA.

- SPECIAL PUBLICATION. Scientific, technical, or historical information from NASA programs, projects, and missions, often concerned with subjects having substantial public interest.

- TECHNICAL TRANSLATION. English-language translations of foreign scientific and technical material pertinent to NASA's mission.

Specialized services that complement the STI Program Office's diverse offerings include creating custom thesauri, building customized databases, organizing and publishing research results . . . even providing videos.

For more information about the NASA STI Program Office, see the following:

- Access the NASA STI Program Home Page at ***http://www.sti.nasa.gov***

- E-mail your question via the Internet to help@sti.nasa.gov

- Fax your question to the NASA Access Help Desk at 301–621–0134

- Telephone the NASA Access Help Desk at 301–621–0390

- Write to:
  NASA Access Help Desk
  NASA Center for AeroSpace Information
  7121 Standard Drive
  Hanover, MD 21076

NASA/CR—2003-212541

A Simple Model of Pulsed Ejector Thrust Augmentation

Jack Wilson
QSS Group, Inc., Cleveland, Ohio

Prepared under Contract NAS3–00145

National Aeronautics and
Space Administration

Glenn Research Center

August 2003

Acknowledgments

The assistance of many people in accomplishing this work is gratefully acknowledged, in particular, Dennis Culley and Daniel Paxson, for the hot-wire measurements; Wentworth John, Dan Paxson, and Mark Wernet, for the LPIV studies; and Robert Pastel and Kevin Dougherty, for the assistance with the experiments.

The Propulsion and Power Program at
NASA Glenn Research Center sponsored this work.

Available from

NASA Center for Aerospace Information
7121 Standard Drive
Hanover, MD 21076

National Technical Information Service
5285 Port Royal Road
Springfield, VA 22100

Available electronically at http://gltrs.grc.nasa.gov

A Simple Model of Pulsed Ejector Thrust Augmentation

Jack Wilson
QSS Group, Inc.
Cleveland, Ohio 44135

Summary

A simple model of thrust augmentation from a pulsed source is described. In the model it is assumed that the flow into the ejector is quasi-steady, and can be calculated using potential flow techniques. The velocity of the flow is related to the speed of the starting vortex ring formed by the jet. The vortex ring properties are obtained from the slug model, knowing the jet diameter, speed and slug length. The model, when combined with experimental results, predicts an optimum ejector radius for thrust augmentation.

Data on pulsed ejector performance for comparison with the model was obtained using a shrouded Hartmann-Sprenger tube as the pulsed jet source. A statistical experiment, in which ejector length, diameter, and nose radius were independent parameters, was performed at four different frequencies. These frequencies corresponded to four different slug length to diameter ratios, two below cut-off, and two above. Comparison of the model with the experimental data showed reasonable agreement. Maximum pulsed thrust augmentation is shown to occur for a pulsed source with slug length to diameter ratio equal to the cut-off value.

Introduction

The current interest in Pulsed Detonation Engines has revived interest in pulsed ejectors, since the latter may potentially increase the thrust, and reduce the noise level, of such engines with little additional hardware. This supposition is based on the few experiments that have been reported in which thrust augmentation from a pulsating jet was measured. Lockwood (1961), using a pulsejet driver, measured thrust augmentations as high as 1.9, with a very short ejector. Binder and Didelle (1975), using a jet interrupted by a butterfly valve, also observed a maximum thrust augmentation ratio of 1.9, but with a much longer ejector. Bertin (1955), also claimed a thrust augmentation ratio of around 2, but gave few details. More recently, Paxson, Wilson, and Dougherty, (2002) have repeated Lockwood's experiment, with similar results, although the optimum ejector was rather longer than was Lockwood's. Wilson and Paxson (2002), using a Hartmann-Sprenger, or resonance, tube to generate a pulsed jet, measured a maximum thrust augmentation of 1.32, and found, as did Paxson, et al., that there was an optimum diameter for the ejector. Early theoretical work by Johnson and Yang (1968) as well as recent efforts by Han (2002) and Marzouk and Wahab (1997) have concentrated on one-dimensional calculations, using the method of characteristics, to explain the mass flow augmentation of pulsed ejectors, without calculating thrust augmentation.

A major feature of any pulsed jet flow is the starting vortex ring (Elder and deHaas, 1952, Das et al., 2001). The core of this ring exhibits pressures significantly below the ambient pressure, which makes it unlikely that it can be represented in a one-dimensional calculation. One objective of this work is to calculate the thrust on an ejector, and hence the thrust augmentation ratio, based on the properties of the vortex ring. The aim is not so much to produce an accurate expression, as to develop a formula which will give some idea as to the parameters which affect ejector performance. In particular, it is of interest to explore whether there is a maximum value of pulsed thrust augmentation.

In addition, experiments to measure pulsed thrust augmentation were made using a shrouded Hartmann-Sprenger tube as the pulsed source. By varying the tube and shroud lengths, four different frequencies were generated. A statistical experiment was designed to explore the effects of ejector length, radius, and nose radius. This was repeated at each frequency. The experimental results are compared with the theoretical estimates.

Description of the Model

Model Outline

For simplicity, as shown in figure 1, the pulsed jet will be assumed to consist of repeated slugs of length L, with constant velocity U, and density ρ, issuing from a tube of diameter D, as would be produced by a piston impulsively started with velocity U and stopping after a stroke L. According to Gharib, Rambod, and Shariff (1998), the slugs will transform entirely into vortex rings, provided $L/D \leq 4$. Above a value of $L/D = 4$, vortex rings will form with circulation equal to that produced at $L/D = 4$, followed by a trailing jet containing the rest of the circulation. Each vortex ring will have a radius R, and a core of 'radius' a. Strictly speaking, the core may not be a circle, therefore does not have a radius. However, it is approximately circular, and what is meant by a, is the square root of the core area divided by π. The vortex rings will propagate downstream, traveling at a speed W, and impact the ejector, producing thrust. Thrust is presumably created by suction on the nose of the ejector. The ejectors used in this study are cylindrical, with an inner radius equal to R_{ej}, and a rounded nose of radius r_n. The trailing edge is tapered, with a blunt end. The resulting flow could create suction at the trailing edge also, thereby canceling the thrust. At this point, it will simply be assumed that this does not happen. Thus the pressure at the trailing edge will be taken to be the ambient pressure, p_∞. With the above assumptions, the force on the ejector is

$$F_{ejector} = 2\pi \int_0^{2r_n} (p(r,t) - p_\infty)(R_{ej} + r)\, \mathrm{d}r \tag{1}$$

in which r is distance in the radial direction at the nose of the ejector, and $p(r,t)$ the pressure on the nose of the ejector, which may be a function of time and radius. The thrust augmentation ratio, α is defined as the thrust of jet plus ejector divided by the thrust of the jet alone, i.e.

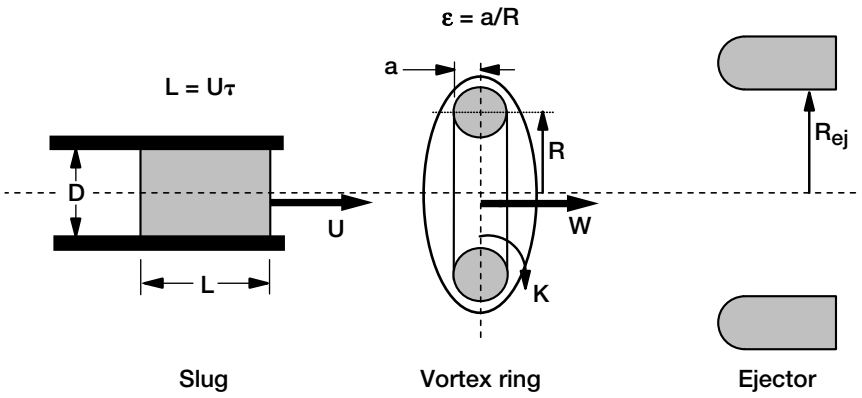

Figure 1.—Schematic diagram of the slug model of vortex ring formation. The entrance to the ejector is also indicated on the right.

$$\alpha = 1 + F_{ejector}/T_{jet} \tag{2}$$

in which T_{jet} is the thrust of the jet itself. In order to evaluate the thrust augmentation further, details of the vortex ring are needed.

Vortex Ring Model

Given the properties of the jet, Linden and Turner (2001) have shown that the properties of the vortex, i.e. R, a, and W, are uniquely determined as a function of the value of L/D for the jet. To demonstrate this, they balanced the jet circulation, impulse and energy with those for the ring, taking the ring values from the work of Norbury (1973). Norbury solved the equations for a vortex ring numerically, at a few values of $\varepsilon = a/R$. Since the interest here is in small values of ε, at several values of this ratio, it is preferable to have a continuous (in ε) representation. Consequently the ring values used will be a modified version of those of Fraenkel (1972), who used a solution as a series in ε, valid for small ε, although in practice, the results agree well with Norbury's values for quite large values of ε. Then with values for the jet in the middle of the equations below, and values for the vortex ring on the right hand side, the balance equations become, using Fraenkel's series representations

$$\text{Circulation: } K_{slug} = U\,L/2\;K_{ring} = \Gamma\,K_{slug} \tag{3}$$

$$\text{Impulse: } P = \pi\,\rho\,UD^2\,L/4 = \pi\,\rho\,R^2\,K_{ring}\,(1 + 3\,\varepsilon^2/4) \tag{4a}$$

$$\text{Energy: } T = \pi\,\rho\,U^2D^2\,L/8 = \rho\,R\,K_{ring}^{\;2}\,[0.5\,\ln(8/\varepsilon) - 7/8 + (3\,\varepsilon^2/16)\,\ln(8/\varepsilon)] \tag{5a}$$

Following Linden and Turner, these equations can be combined to give

$$(L/D)\,\Gamma^{1.5} = \sqrt{\frac{1}{2}\,\pi\left(P/\rho\,R^2\;K_{ring}\right)}/\left(T/\rho\,RK_{ring}^{\;2}\right) \tag{6a}$$

$$= \pi\,\sqrt{\left(1+3\,\varepsilon^2/4\right)}/\left[0.5\,\ln\left(8/\varepsilon\right) - 7/8 + \left(3\,\varepsilon^2/16\right)\ln\left(8/\varepsilon\right)\right] \tag{6b}$$

The right hand side of this equation, and hence L/D also, is a function of ε only. In order to agree better with Norbury's values of impulse and energy, the above series were modified to

$$P_{ring} = \pi\,\rho\,R^2\,K_{ring}\,(1 + 0.303\,\varepsilon + 0.6184\,\varepsilon^2 - 0.3563\,\varepsilon^3) \tag{4b}$$

$$T_{ring} = \rho\,R\,K_{ring}^{\;2}\,[0.5\,\ln(8/\varepsilon) - 0.8594 + 0.098\,\varepsilon^2\,\ln(8/\varepsilon)] \tag{5b}$$

In figure 2(a), L/D is plotted against ε using (4b) and (5b) in (6a), with $\Gamma = 1$, as assumed by Linden and Turner. Also shown are results from Linden and Turner for $\varepsilon = 0.2$, 0.4, and 0.6. The agreement is quite good, even for $\varepsilon = 0.6$. The limiting value of $L/D = 4$ is found at a value of $\varepsilon = 0.55$, so higher values of ε than this are not needed.

It was implicitly assumed above that U was a constant independent of time. This is rarely true in practice. If the actual temporal distribution of velocity from the source is represented by $u(t)$ then it follows that $L = \int u(t)\,dt$, and the jet circulation, impulse and energy are

$$K_{slug} = \int u(t)^2\,dt/2 = U_1L/2 \tag{7a}$$

$$P = \pi \rho D^2 L/4 \left(\int u(t)^2\, dt / \int u(t)\, dt\right) = \pi \rho D^2 L\, U_1/4 \tag{7b}$$

$$T = \pi \rho D^2 L/8 \left(\int u(t)^3\, dt / \int u(t)\, dt\right) = \pi \rho D^2 L\, U_2{}^2/8 \tag{7c}$$

and the right hand side of (6a) is now multiplied by $(U_2/U_1)^2$.

Combining (3) and (4b) leads to an equation for R/D in terms of ε, and hence, through (6a), L/D.

$$R/D = 1/\sqrt{2\Gamma\left(1 + 0.303\,\varepsilon + 0.6184\,\varepsilon^2 - 0.3563\,\varepsilon^3\right)} \tag{8}$$

Fraenkel's equation for the vortex ring velocity, W, is

$$W = (K_{ring}/4\pi R)\left[\ln(8/\varepsilon) - 1/4 - \varepsilon^2\left\{(3/8)\ln(8/\varepsilon) - 15/32\right\}\right] \tag{9a}$$

which fits the calculated results of Norbury better if modified to

$$W = (K_{ring}/4\pi R)\left[\ln(8/\varepsilon) - 1/4 - 0.85\,\varepsilon^2\left\{(3/8)\ln(8/\varepsilon) - 15/32\right\}\right] \tag{9b}$$

and using (3) and (8), the ring velocity divided by the slug velocity is seen to be a function of L/D and ε only,

$$W/U = \Gamma^{1.5}(L/D)\sqrt{2\left(1 + 0.303\,\varepsilon + 0.6184\,\varepsilon^2 - 0.3563\,\varepsilon^3\right)} \times \left|\ln(8/\varepsilon) - 1/4 - 0.85\,\varepsilon^2\left\{(3/8)\ln(8/\varepsilon) - 15/32\right\}\right|/8\pi \tag{10}$$

and hence can also be expressed in terms of L/D. R/D and W/U, again for $\Gamma = 1$, are also plotted against L/D in figure 2(a). W/U agrees well with results from Linden and Turner. However, the calculated values of R/D do not agree with experimental values of R/D from Liess and Didden (1975) in the dependence on L/D. The calculated values decrease with increasing L/D, whereas the experimental values increase.

Shariff and Leonard (1992) have plotted ring circulation divided by slug circulation, i.e. Γ against L/D, using data from Didden (1979), and from Maxworthy (1977), and find that this ratio is not unity, and decreases with increasing L/D. They quote two expressions for Γ, but neither fits all the data. Both are close at $L/D = 1$, with $\Gamma = 1.4$, which does give the experimental value of R/D found by Liess and Didden. By finding a value of Γ that fits the Liess and Didden value of R/D at $L/D = 2.5$, the constants in the following expression were found,

$$\Gamma = K_{ring}/K_{slug} = 0.66 + 0.74/(L/D) \tag{11}$$

This agrees with the two expressions quoted by Shariff and Leonard at $L/D = 1$, and falls between them at $L/D = 2.5$, so it does not seem unreasonable. Using Γ from (11), ε, R/D, and W/U were calculated, and are plotted in figure 2(b). Now there is excellent agreement between the calculated R/D and the experimental values of Liess and Didden.

In summary, given the slug velocity, length and diameter, the vortex ring circulation, radius, and core radius, and hence velocity, can all be determined, but it is essential to input Γ as a function of L/D.

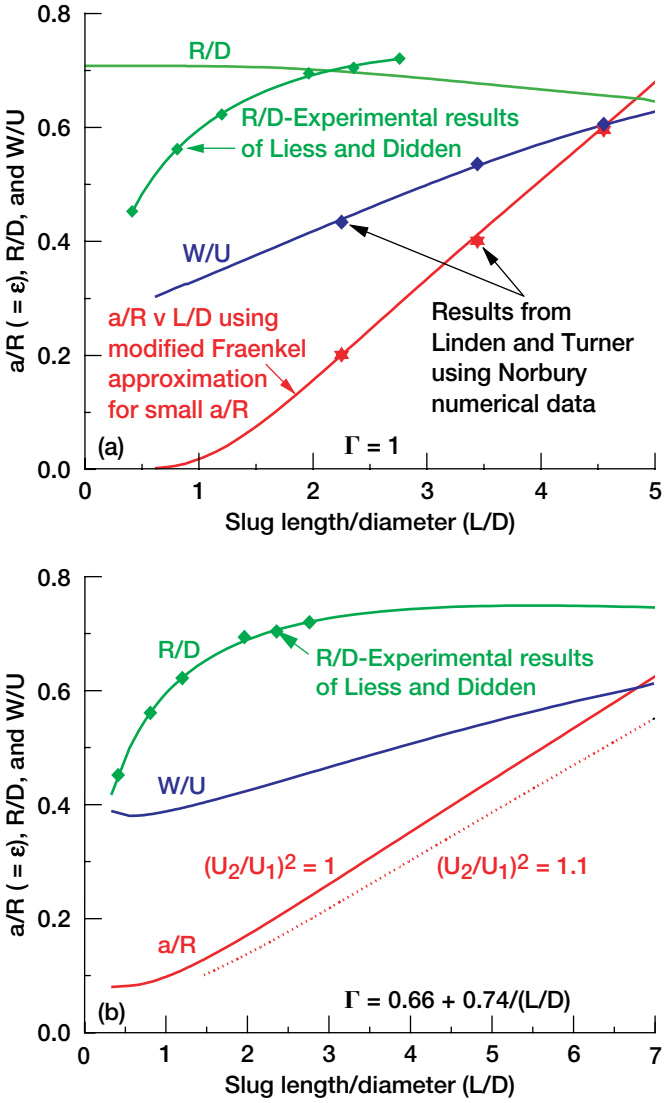

Figure 2.—Calculations of ε, R/D and W/D using the slug model. (a) With Γ = 1. (b) With Γ = 0.66 + 0.74/(L/D).

Force on the Ejector

The exact flow of a vortex ring approaching an ejector is complex, and depends on the ratio of vortex ring size to ejector radius. Krutzsch (1939) reports passing rings through tubes 'of diameter somewhat greater than that of the vortex ring', although doing so increased the vortex ring decay rate. On the other hand, calculations and experiments by Brasseur (1979) indicate that a vortex ring will not propagate inside a tube of radius close to that of the vortex ring. For now it will be assumed that the net result of a repetitive stream of vortex rings approaching an ejector is the setting-up of a quasi-steady flow characterized by a centerline velocity V_{ej} inside the ejector, whose value is as yet unknown. Thus to calculate the force on the ejector, if the flow field around the nose can be calculated, the pressures can be determined, and integrated to give the force. The nose piece of all ejectors used in this study were half of a ring of cross-sectional radius r_n. Flow around a complete ring is, of course, the same as flow around the core of a vortex ring, provided the cross-sectional radius of the ring is small compared with the radius of

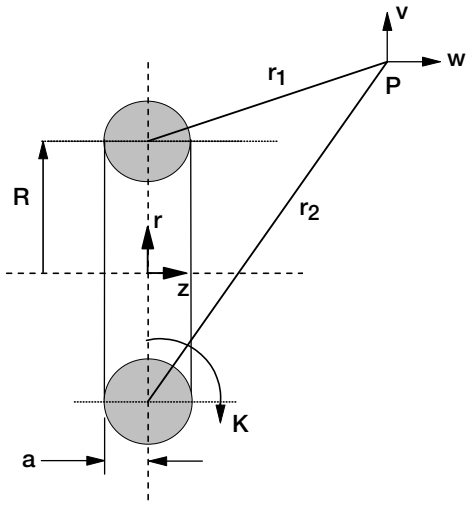

Figure 3.—Coordinate system for the vortex ring.

the ring itself, i.e. $r_n < R_{ej}$. It will be assumed that the flow over the ejector nose can be approximated by the inlet flow around a vortex ring. For a vortex ring of circulation K_{ring}, a stream function exists, given by Lamb (1932) as

$$\psi(r,z) = -K_{ring}\,(r_1 + r_2)\,\{F_1(\lambda) - E_1(\lambda)\}/2\pi \qquad (12)$$

where

$$\lambda = (r_2 - r_1)/(r_2 + r_1)$$

and $F_1(\lambda)$, $E_1(\lambda)$ are the complete elliptic integrals of the first and second kind. The radii r_1 and r_2 are the minor and major distances from the point (z,r) to the core ring (see fig. 3). Since this is axisymmetric flow, the axial and radial velocities are given by

$$w = (1/r)\,\partial\psi/\partial r \qquad v = -(1/r)\,\partial\psi/\partial z \qquad (13)$$

and then, for example,

$$\partial\psi/\partial r = -(K_{ring}/2\pi)[\,\{F_1(\lambda) - E_1(\lambda)\}\;\partial/\partial r\,(r_1 + r_2) + (r_1 + r_2)\;\mathrm{d}/\mathrm{d}\lambda\{F_1(\lambda) - E_1(\lambda)\}\partial\lambda/\partial r] \qquad (14)$$

with a similar equation for $\partial\psi/\partial z$. From Gradshteyn and Ryzhik (1994),

$$\mathrm{d}/\mathrm{d}\lambda\{F_1(\lambda) - E_1(\lambda)\} = \lambda\,E_1(\lambda)/(1 - \lambda^2) \qquad (15a)$$

and

$$F_1(\lambda) - E_1(\lambda) = \lambda^2\,D(\lambda) \qquad (15b)$$

Gradshteyn and Ryzhik also list series representations of $E_1(\lambda)$ and $D(\lambda)$. With these series, and the above formulae, a program was written to calculate ψ, w and v (for a given K_{ring}) at any point (r,z). A version of this program was made to solve for r and z for a constant value of ψ, i.e. to find the streamlines. These streamlines then constitute potential solid bodies around which flow can occur. Examples are given in figure 4. With the velocities known at each point on any surface, the pressure follows from Bernoulli's equation

$$p_{(\psi\,=\,const)} - p_\infty = 0.5\,\rho\,(w^2 + v^2) \qquad (16)$$

Performing the integral

$$F_{ejector} = 2\pi \int_{R_{ej}}^{R_{ej}+2r_n} (p(r,z) - p_\infty)\,r\,\mathrm{d}r \qquad (17)$$

provides the suction force, F_{ej}, on the front of the ejector, and hence, if it is assumed that the rear of the ejector is at atmospheric pressure, the total force on the ejector. Obviously frictional drag has been ignored. Inserting (16) into (17), and re-arranging gives

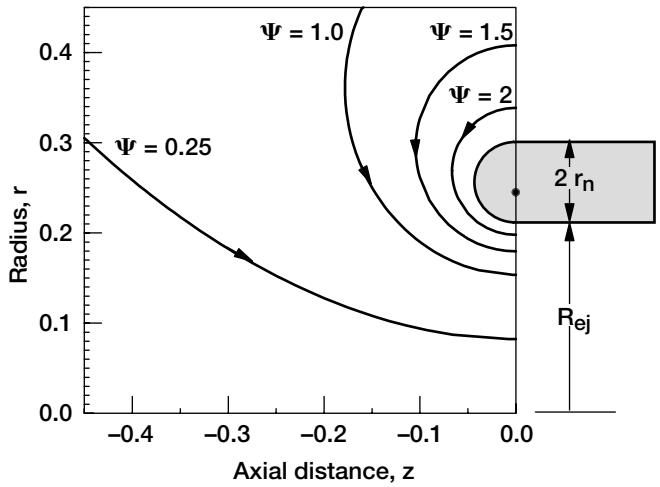

Figure 4.—Streamlines in the z-r plane through a vortex ring. The streamline for $\Psi = 2.5$ has been taken as the nose of an ejector with nose radius r_n.

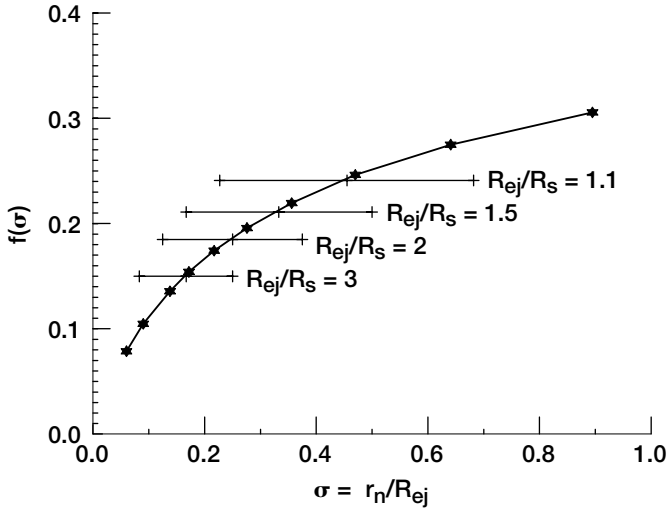

Figure 5.—The function f(σ) versus σ. The horizontal lines are drawn through the values of σ used for each ejector.

$$F_{ejector} = \pi \rho V_{ej}^2 R_{ej}^2 \int_1^{1+2r_n/R_{ej}} ((w^2 + v^2)/V_{ej}^2)(r/R_{ej})\, dr/R_{ej} \tag{18a}$$

$$= \pi \rho V_{ej}^2 R_{ej}^2 F(\sigma) \tag{18b}$$

where $\sigma = r_n/R_{ej}$. If V_{ej} is taken to be the centerline velocity, the integral is dimensionless, a function of σ only, and can be determined from the calculations of velocities that gave the results in figure 4. $F(\sigma)$ is plotted in figure 5. A useful fit to $F(\sigma)$ is

$$F(\sigma) = 0.0236 + 1.0621\,\sigma - 2.1468\,\sigma^2 + 2.3689\,\sigma^3 - 1.0074\,\sigma^4 \tag{19}$$

Finally, the thrust augmentation due to the vortex ring can now be given as

$$\alpha_{vr} = 1 + \pi \rho V_{ej}^2 R_{ej}^2 F(\sigma)/T_{jet} \tag{20}$$

Determination of V_{ej}

In order to use eq. (20), it is necessary to know the value of V_{ej}. A characteristic size of the vortex ring will be denoted R_{vr}, which will be approximately equal to $R + a$. Since the vortex rings are approaching the ejector with velocity W, it seems reasonable, if $R_{ej} < R_{vr}$, that the velocity V_{ej} should be close to W. It will be assumed to be proportional to it, i.e. $V_{ej} = k\,W$. If, on the other hand, $R_{ej} > R_{vr}$, the vortex rings will travel through the ejectors as 'leaky pistons,' with a resulting net lower value of V_{ej}. Without an ejector, for a vortex ring traveling to the right at speed W, since the air traveling with the vortex ring is approximately an ellipsoid, the velocity on a radius through the center of the vortex for distances larger than R_{vr} will be approximately that for an ellipsoid

$$w = -\,W/2\,(R_{vr}/r)^3 \tag{21}$$

and the flux of air to the left in a disc of inner radius $(R + a)$, and outer radius R_{ej}, is

$$Q_L = -\,(W/2)\int_{R_{vr}}^{R_{ej}} (R_{vr}/r)^3\, 2\pi r \mathrm{d}r \tag{22a}$$

$$= -\,\pi\, W\,(R_{vr})^3\,[1/R_{vr} - 1/R_{ej}] \tag{22b}$$

The vortex ring itself will create a flux of air to the right of

$$Q_R = W\,\pi\,R_{vr}^{\,2} \tag{23}$$

So that the net flux inside a cylinder of radius R_{ej} is

$$Q_{total} = Q_R + Q_L \tag{24a}$$

$$= \pi\, W\, R_{vr}^{\,3}/R_{ej} \tag{24b}$$

and the average velocity inside the cylinder is then

$$V_{ej} = Q_{total}/\pi\,R_{ej}^{\,2} \tag{25a}$$

$$= W\,[R_{vr}/R_{ej}]^3 \tag{25b}$$

Obviously, this formula is only approximately correct, but at least it is correct in the limit of $R_{ej} = R_{vr}$, for which $V_{ej} = W$, and also in the limit as R_{ej} tends to infinity, for which $V_{ej} = 0$. This would also be true for any expression of the form

$$V_{ej} = k\,W\,[R_{vr}/R_{ej}]^n \tag{26}$$

This is the velocity that will be used in eq. (19) when $R_{ej} > R_{vr}$. The values of n and k will be found from the experiment. Given V_{ej}, the mass augmentation factor β can be calculated as

$$\beta = \rho\,\pi\,R_{ej}^{\,2}\,V_{ej}/\dot{m}_{jet} \tag{27}$$

in which $\dot{m}_{jet}$ is the mass flow of the jet itself.

Pulsed Jet Source

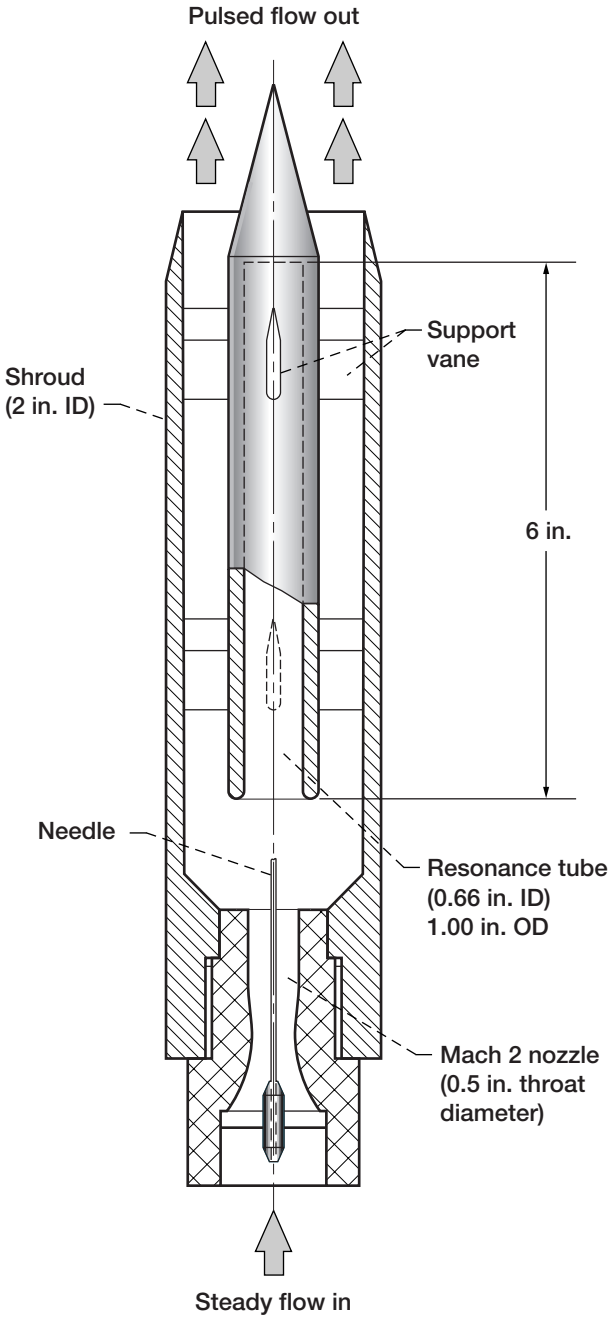

Figure 6.—Schematic drawing of the shrouded Hartmann-Sprenger tube.

In deciding upon an experiment, it is necessary to choose a source producing a pulsed jet. Since a major interest for studying pulsed ejectors is for application to pulsed detonation engines, the optimum source would be a pulsed detonation device. Such devices, particularly with long duration, are not simple to build and operate. In contrast, a resonance, or Hartmann-Sprenger tube (Brocher, 1975), is simple, and can operate continuously. This device consists of a steady, sonic or supersonic jet, which is flowing into a closed tube. Under certain conditions, a periodic cycle is established in which the jet first fills the tube, then a hammer shock inside the tube empties the tube, deflecting the jet from the tube in the process. When the tube pressure has fallen sufficiently, the cycle can begin again. What was not known at the start of this effort was whether this phenomenon could also produce a directed, pulsed jet. To attempt this, a cylindrical shroud was placed around the tube and jet, to collect the air leaving the tube and direct it out the back of the shroud. Resonance tubes have been shrouded previously (Brocher and Pinna, 1980), but with acoustic horns, with the objective of amplifying the sound. These acoustic horns were closed at the end where the source is located, and increased in area with distance away from the source. The flow from the horn would therefore be diverging, and the velocity at the exit would be reduced in value from that leaving the source. In order to create a more concentrated flow, a cylindrical shroud was used in the present work. This shrouded tube did produce vortex rings traveling along the extended axis of the device

The shrouded tube used at a frequency of 550 Hz is shown in figure 6. A Mach 2 axisymmetric nozzle with a 12.7 mm diameter throat was aligned with a resonance tube 152 mm in length, internal diameter 16.8 mm, and external diameter, d_t = 25.4 mm. This was surrounded by a shroud, of internal diameter D_s = 50.8 mm. A needle was aligned with the axis of the jet to stimulate oscillations, as demonstrated by Brocher. Use of the needle makes the device relatively insensitive to the distance between nozzle exit and the tube entrance. A supply of air at a pressure of 7.8 atmospheres ensured Mach 2 operation exhausting to the atmosphere. The average mass flow was measured upstream of the nozzle, using an orifice. In order to generate a frequency of 1100 Hz, a plug was inserted into the resonance tube, effectively shortening it to 76 mm in length. New, longer tubes and shrouds were built for frequencies of 275 and 125 Hz.

Design of the Experiment

The unsteady experiments to date in which thrust augmentation was measured for a pulsating jet, namely those of Lockwood (1961), and Binder and Didelle (1975), have each shown a peak of thrust augmentation at some value of L/D, with an approximately parabolic distribution of augmentation about that peak. Thus it is appropriate to use a statistical design with a 3 level set of parameters in the experiment. There are many parameters that can affect the performance of an ejector, e.g. ejector length, ejector radius, distance from jet exit to ejector entrance, ejector geometry, ratio of jet temperature to entrained air temperature, jet frequency, and details of the driving pulse (i.e. pulse amplitude, duration, and temporal distribution, and frequency). By fixing the frequency of the driving jet, having it produce an invariant pulse, and not heating the air supplying the jet, the list is reduced somewhat, although obviously at the cost of not determining the effect of these now fixed parameters. Of the remaining variables, ejector length, radius and nose radius were chosen as independent parameters. The distance from jet exit to ejector entrance was treated as a dependant parameter, i.e. it was varied for each ejector combination until a maximum value of thrust augmentation was found. A three parameter, three level Box-Behnken design (Mason, Gunst, and Hess, 1989) was chosen for the experiment. After a set of runs at one frequency, the tube and shroud were altered, i.e. lengthened or shortened, to give a different frequency, and a new set of runs made. Four frequencies were used, 1100, 550, 275, and 125 Hz.

In order to achieve the three parameter, three level, test matrix, a set of ejectors was built as shown in figure 7, consisting of entrance sections, center sections, and a diffusing tail section. At each ejector radius, three nose sections were made, each of a different nose radius, r_n, two center sections of different length, and one tail section. By using either no center section, a short center section, or a long one, three different lengths of ejector, L_{ej} were obtained, roughly 76, 190, and 318 mm. Since prior experiments with steady ejectors have shown that thrust augmentation increases with the ratio of exhaust area to jet area (Porter and Squyers, 1979), with values as high as 100 having been used, it appeared that the experiment should include large ejector radius to jet radius ratios. Consequently, ratios of ejector throat radius, R_{ej}, to jet shroud radius, R_s, of 1.5 (R_{ej} = 38 mm), 3 (R_{ej} = 76 mm), and 4.5 (R_{ej} = 114 mm) were chosen. Experiments at a frequency of 550 Hz with the ratios 1.5 and 3 soon showed that the optimum augmentation was at a ratio less than 3. Instead of pursuing the experiments with the radius ratio 4.5 ejectors, new sets at radius ratios of 1.1 and 2 were made. The test matrix used is given in table 1, with runs 1 through 15 constituting the design for 1100 and 550 Hz, and runs 20 through 28 the design for 275 and 125 Hz. Runs 16 through 19 are the runs performed at 550 Hz with R_{ej}/R_s = 3.

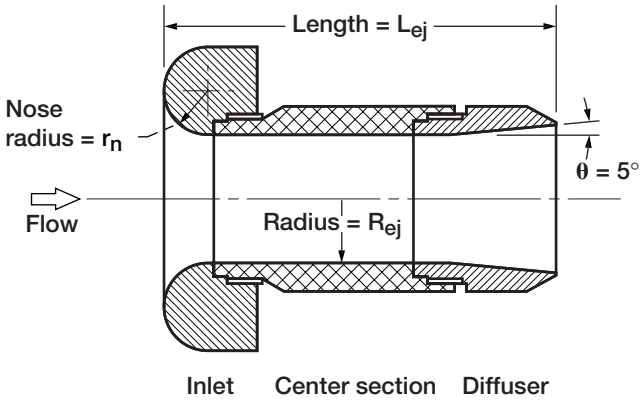

Figure 7.—Schematic drawing of the set of ejectors used experimentally.

In these experiments, the objective was measurement of thrust augmentation. However, an ejector also results in mass augmentation, and it is of interest to correlate thrust augmentation and mass augmentation. A hot wire, used to measure velocity in the ejector exit flow provided a means for calculating entrainment ratio. Details are given below.

Table 1.—The matrix of test runs comprising the 3 parameter, 3 level statistical experiment at each of the four frequencies used

Run No.	R_{ej}/R_s	L_{ej}/R_s	r_n/R_s	α				β
				f = 1100	f = 550	f = 275	f = 125	f = 550
1	1.1	3.125	0.5	1.17	1.155			
2	1.1	7.125	0.25	1.149	1.16			0.897
3	1.1	7.625	0.75	1.134	1.155			
4	1.1	12.375	0.5	1.122	1.092			
5	1.5	2.875	0.25	1.099	1.264			
6	1.5	3.375	0.75	1.053	1.275			
7	1.5	7.375	0.5	1.172	1.330			
8	1.5	7.375	0.5	1.167	1.325			1.895
9	1.5	7.375	0.5	1.169	1.308			
10	1.5	12.125	0.25	1.166	1.255			
11	1.5	12.625	0.75	1.165	1.267			
12	2	3.125	0.5	1.022	1.118			
13	2	7.125	0.25	1.092	1.206			
14	2	7.625	0.75	1.10	1.226			
15	2	12.375	0.5	1.167	1.266			
16	3	3.125	0.5		1.034			
17	3	7.125	0.25		1.075			
18	3	7.625	0.75		1.085			
19	3	12.375	0.5		1.139			
20	1.5	3.125	0.5			1.287	1.14	
21	1.5	7.125	0.25			1.320	1.221	
22	1.5	7.625	0.75			1.355	1.237	
23	1.5	12.375	0.5			1.326	1.265	
24	2	2.875	0.25			1.277	1.186	
25	2	3.375	0.75			1.343	1.218	
26	2	7.375	0.5			1.379	1.317	
27	2	7.375	0.5			1.373	1.295	
28	2	7.375	0.5			1.376	1.313	
29	2	12.125	0.25			1.305	1.271	
30	2	12.625	0.75			1.383	1.310	
31	3	3.125	0.5			1.053	1.075	
32	3	7.125	0.25			1.106	1.137	
33	3	7.625	0.75			1.116	1.182	
34	3	12.375	0.5			1.197	1.250	

Apparatus

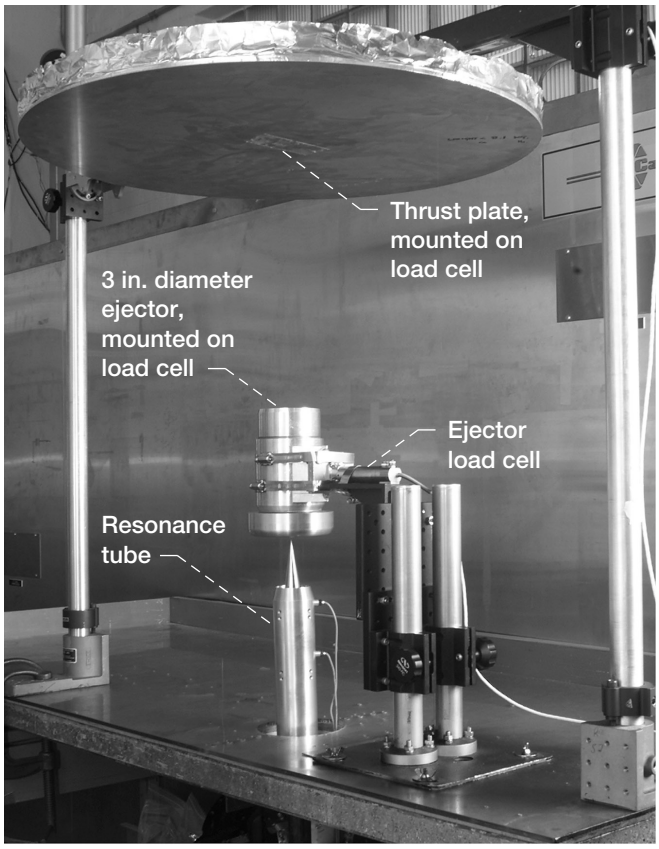

Figure 8.—Photograph of the apparatus, showing the thrust plate at the top, the shrouded Hartmann-Sprenger tube at the bottom, and an ejector above it.

The apparatus is shown in figure 8. The Hartmann-Sprenger tube is mounted vertically, with the jet flowing upwards. The ejector is mounted above the tube, on a sliding mount so that its height is easily adjustable. Above the ejector is a thrust plate, which is 762 mm in diameter. The thrust plate is attached to an Omega load cell model LC601–25, having a range of ± 111 Newtons, to provide an electrical thrust signal. Similarly the ejector was attached to another load cell, also a model LC601–25. The signal from both load cells was fed to Agilent model 34401A averaging multimeters. All runs lasted one minute, during which time the voltmeters stored 180 readings, and then displayed the average value. The experimental procedure involved making three tests to read the thrust of the jet without the ejector, followed by a series of tests with the ejector, (two at each setting of jet exit to ejector distance), followed again by three tests reading the thrust of the jet without an ejector. The jet thrust, T_{jet}, defined as the average of the six test readings without the ejector, typically measured 39.4 ± 0.5 Newtons. The signal from the ejector load cell corresponds to the additional thrust, ΔT, produced by the ejector. Thus the quantity ϕ, defined as

$$\phi = 1 + \Delta T/T_{jet} \tag{28}$$

should be the same as the thrust plate measurement of thrust augmentation, α. The estimated uncertainty in the measurements of both α and ϕ is ± 0.03.

In addition to thrust augmentation, it is desirable to measure mass flow augmentation. For this, measurements of the jet mass flow and the mass flow leaving the ejector are needed. Since the Mach 2 nozzle in the resonance tube is choked, the jet mass flow can be measured upstream of the nozzle, where it will be a steady reading. For this a standard orifice was mounted in the supply line to the jet. The jet flow was measured both as a steady supersonic flow, i.e. with the resonance tube removed, and with the resonance tube in place. The resulting mass flow was indeed identical for the two cases, with a value of 0.208 ± 0.001 Kg/sec. For measuring the mass flow at the exit of the ejector, two techniques were implemented; first, probing the flow with a high frequency pressure transducer (Endevco model 8530C–50), mounted in the hemispherical nose of a cylinder; and second, probing the flow with a Thermal Systems Inc. model IFA 300 hot-wire, which provided the radial distribution of velocity at the ejector exit.

Obviously it is of interest to measure the properties of the vortex rings produced, namely velocity, radius and core radius, for comparison with the slug model theory. To do this, the rings were probed with a pair of fast response transducers (Endevco model 8530C–50) each built into the nose of a hemisphere-

cylinder body, and separated radially by a distance of 25.4 mms. The probes were inserted into the flow at the same distance from the jet exit as the entrance to the 38 mm radius, 188 mm long, 12.7 mm nose radius ejector at its optimum spacing, i.e. the spacing giving maximum thrust augmentation, which was 76 mm for this ejector. The signals from the probes were displayed on an oscilloscope, using dc coupling. The pair was moved radially to generate a plot of pulse pressure versus radius for the vortex rings. This information gave an indication of the vortex radius and core radius. Then, by spacing the probes equidistantly from the jet axis, at a radius at which the probes gave the minimum pressure signals (the minima being sharper than the maxima), but separating the probes axially, a measurement of the vortex ring velocity could be made. This was repeated for each frequency. For the 275 Hz frequency only, a laser particle image velocimeter (LPIV), as described by John, Paxson, and Wernet (2002), was used to give a velocity map of the vortex ring. One of the high frequency pressure probes was also placed at the jet exit to obtain the jet exit velocity as a function of time.

Experimental Results

Thrust Augmentation

In figure 9 are shown measurements of thrust augmentation, α, versus the jet exit to ejector entrance distance, x, normalized by R_s, for the 38 mm radius ejector (R_{ej}/R_s = 1.5). The results are typical of all the ejectors: thrust augmentation has a maximum at some distance, which depends mainly on the diameter of the ejector, falling off slowly as distance increases beyond the maximum, but quite rapidly as distance decreases below the maximum. The maximum value of ϕ, the thrust augmentation derived from the ejector load cell reading, occurs at lower values of x than does α. This may be due to a decrease in the jet thrust when x is small or negative, which is reflected in the measurement of α, but not of ϕ as defined above. At the maximum of augmentation however, and for larger values of x, both α and ϕ are in good agreement. In the remainder of this work, the thrust augmentation ascribed to a particular ejector is the maximum value of α.

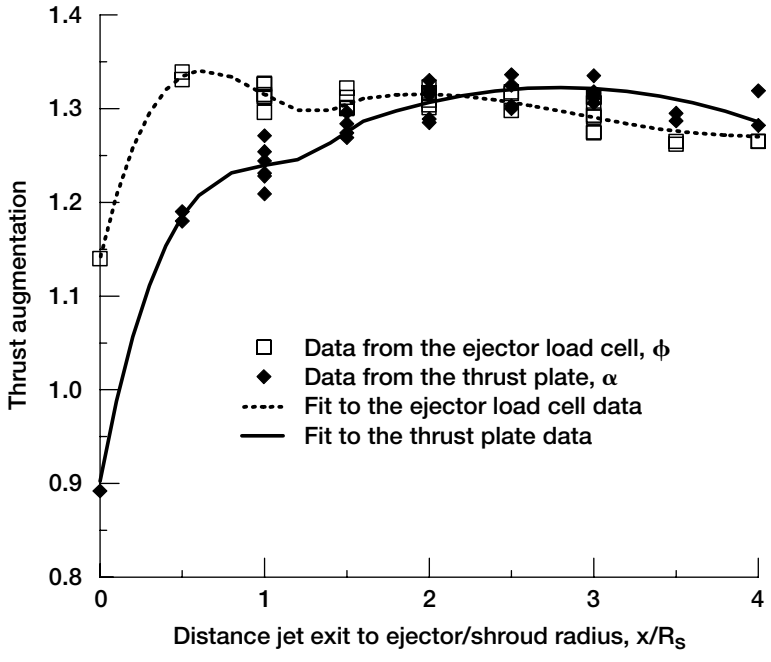

Figure 9.—Thrust augmentation plotted against the distance between the jet exit and the ejector entrance.

The measurements of thrust augmentation found in the various sets of Box-Behnken runs are given in table 1, and in figure 10(a) to (d), in which thrust augmentation is plotted against normalized ejector length, L_{ej}/R_s, for each ejector radius, R_{ej}, at different values of the nose radius, r_n. The 90 percent confidence level in α is ± 0.03. The data from a Box-Behnken three parameter set can be fitted with a response surface of the form

$$\alpha = b_0 + b_1.(L_{ej}/R_s) + b_2.(R_{ej}/R_s) + b_3.(r_n/R_s) + b_{11}.(L_{ej}/R_s)^2 + b_{22}.(R_{ej}/R_s)^2 + b_{33}.(r_n/R_s)^2 + b_{12}.(L_{ej}.R_{ej})/R_s^2 + b_{13}.(L_{ej}.r_n)/R_s^2 + b_{23}.(R_{ej}.r_n)/R_s^2 \quad (29)$$

where the values of the constants b_{ij} are determined from the data. These were found by inserting the data into a computer program (Seshadri and Demming), which provides the constants, and values of the confidence level for each constant. Constants with low confidence level were eliminated, until only terms with levels greater than 90 percent were retained. The resulting constants are listed in table 2. Once the response surface is known, the optimum thrust augmentation can be predicted, together with the values of L_{ej}/R_s, R_{ej}/R_s and r_n/R_s at which the optimum occurs. These values are also listed in table 2.

Although (29) includes r_n, changes in α due to changes in r_n for the range of values used are very small, and the changes seen experimentally are statistically insignificant, except possibly for $r_n/R_s = 0.25$, $R_{ej}/R_s = 2$, at a frequency of 275 Hz.. Sections through the response surface at each value of ejector radius, R_{ej}, for $r_n/R_s = 0.5$, are also plotted in figure 10, showing good agreement with the experimental results. The optimum values predicted are little different from the maximum observed experimental values.

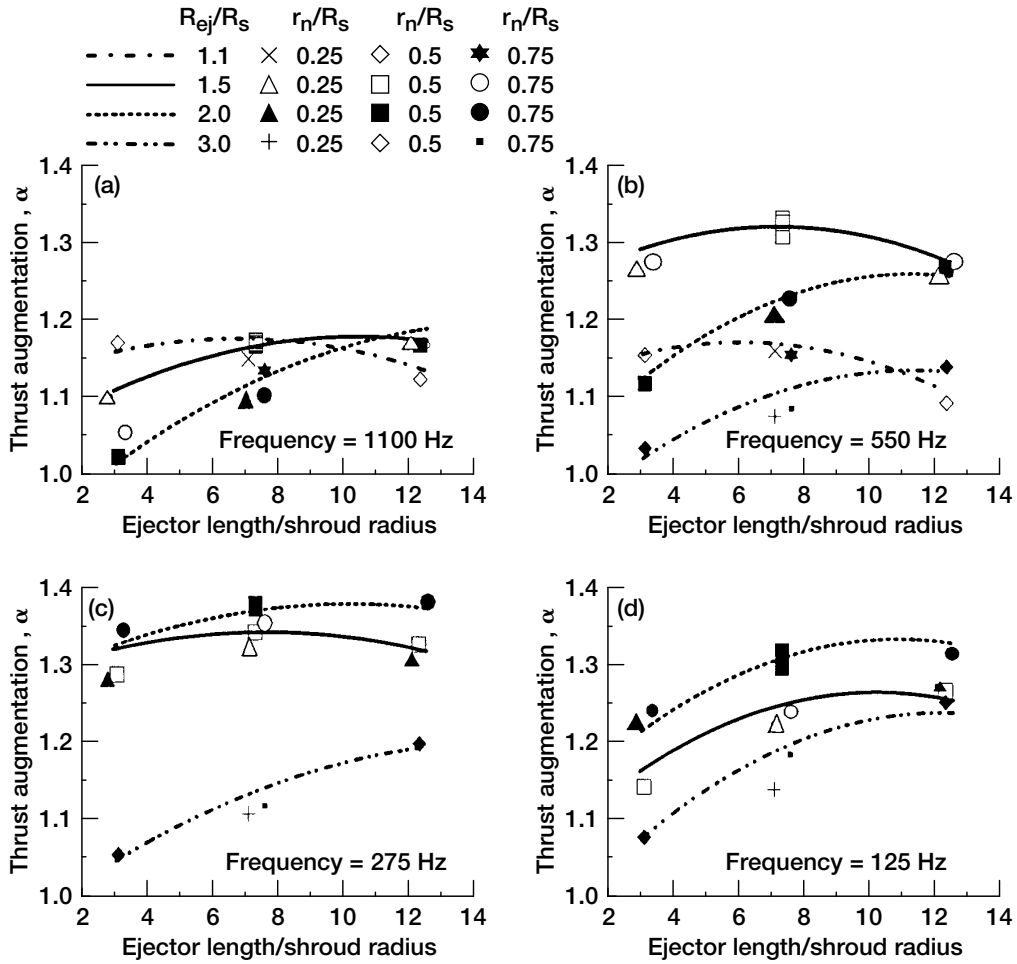

Figure 10.—Results from the statistical experiments at different frequencies. (a) 1100 Hz. (b) 550 Hz. (c) 275 Hz. (d) 125 Hz. The lines are the response surface fit for $r_n/R_s = 0.5$.

Table 2.—Constants for (29)—the response surface of the Box-Behnken experimental design

	f = 1100 Hz	f = 550 Hz	f = 275 Hz	f = 125 Hz
b_0	1.16812	–0.18464	0.54744	0.32863
b_1	–0.01464	–0.00713	--	0.03207
b_2	--	1.81433	0.68699	0.64294
b_3	0.28836	0.23637	0.52521	0.44842
b_{11}	–0.00126	–0.00197	–0.00103	–0.00193
b_{22}	–0.07511	–0.62527	–0.19356	–0.15947
b_{33}	–0.41306	–0.21744	–0.30355	–0.39603
b_{12}	0.02336	0.02591	0.01052	0.00505
b_{13}	0.01187	--	--	
b_{23}	--	--	–0.06310	
α_{max}	1.189	1.331	1.385	1.338
R_{ej}/R_s for α_{max}	1.98	1.62	1.91	2.21
L_{ej}/R_s for α_{max}	12.6	8.9	9.9	11.2
r_n/R_s for α_{max}	0.5	0.5	0.75	0.5

Vortex Ring Probing

Signals from the high frequency pressure probes sampling the vortex rings at a distance (usually 76 mm) from the nozzle exit, are shown in the oscillogram in figure 11(a), taken at a frequency of 550 Hz, As indicated in the sketch in figure 11(b), two probes were used, both aligned with the z axis, and spaced 25.4 mm apart. The upper oscillogram is from the probe closer to the axis of the jet, and exhibits a rise in pressure with time, followed by a decay, returning to atmospheric pressure at about half the period of the pulses. After the signal returned to atmospheric, there appeared to be a high frequency oscillation on it, lasting until the next pulse. As the probe was moved radially, away from the jet axis, the value of the peak pressure first increased slightly, then decreased to zero at a radial position equal to about 1.2 times the jet radius. At distances greater than this, a pulse was seen which was a decrease in pressure, with a minimum pressure well below atmospheric, as shown by the lower oscillogram in figure 11(a), which is from the probe further from the axis. The values of the pulse extrema, expressed as pressures, are plotted as a function of distance from the jet axis in figure 11(b). For a frequency of 550 Hz, the absolute outer edge of the disturbance, where there is no longer any signal, is at a radial position of 3.2 times the jet radius, i.e. 81 mm, much larger than the optimum ejector radius. The optimum ejector radius corresponds approximately to the position of the minimum of the negative pressure signals, i.e. 1.5 times the jet exit radius at a frequency of 550 Hz. These measurements were repeated at each frequency used.

The positive signals are generated when the probe is acting as a Pitot probe, with flow directed towards the transducer. The negative signals are partly generated when the probe is in the core of the vortex ring, such that the flow is in the opposite direction, and the probe is acting more like a static pressure probe. This will become more obvious below.

As stated above, in order to measure the vortex ring velocity, W, the probes were separated axially by a distance varying between 50 to 100 mm, depending on the frequency, and were each at a radial distance from the axis such that they were sampling the pressure minima. Velocities derived from these signals are given in table 3. Each velocity is an average of about 15 readings. Some variation in velocity with probe axial separation, and with position of the leading probe relative to the nozzle exit, was observed, but was less than the experimental error. Also listed in table 3 are the values of the thrust of the jet alone for each frequency. The thrust was not the same at each frequency used, although the mass flow was. This implies that the jet exit velocity U was not the same for each frequency. Since the vortex ring velocity is proportional to U, it is appropriate for comparison to correct the vortex ring velocity to a common thrust of 39.4 Newtons by multiplying the observed value of W by $39.4/T_{jet}$. The corrected values are also given in table 3.

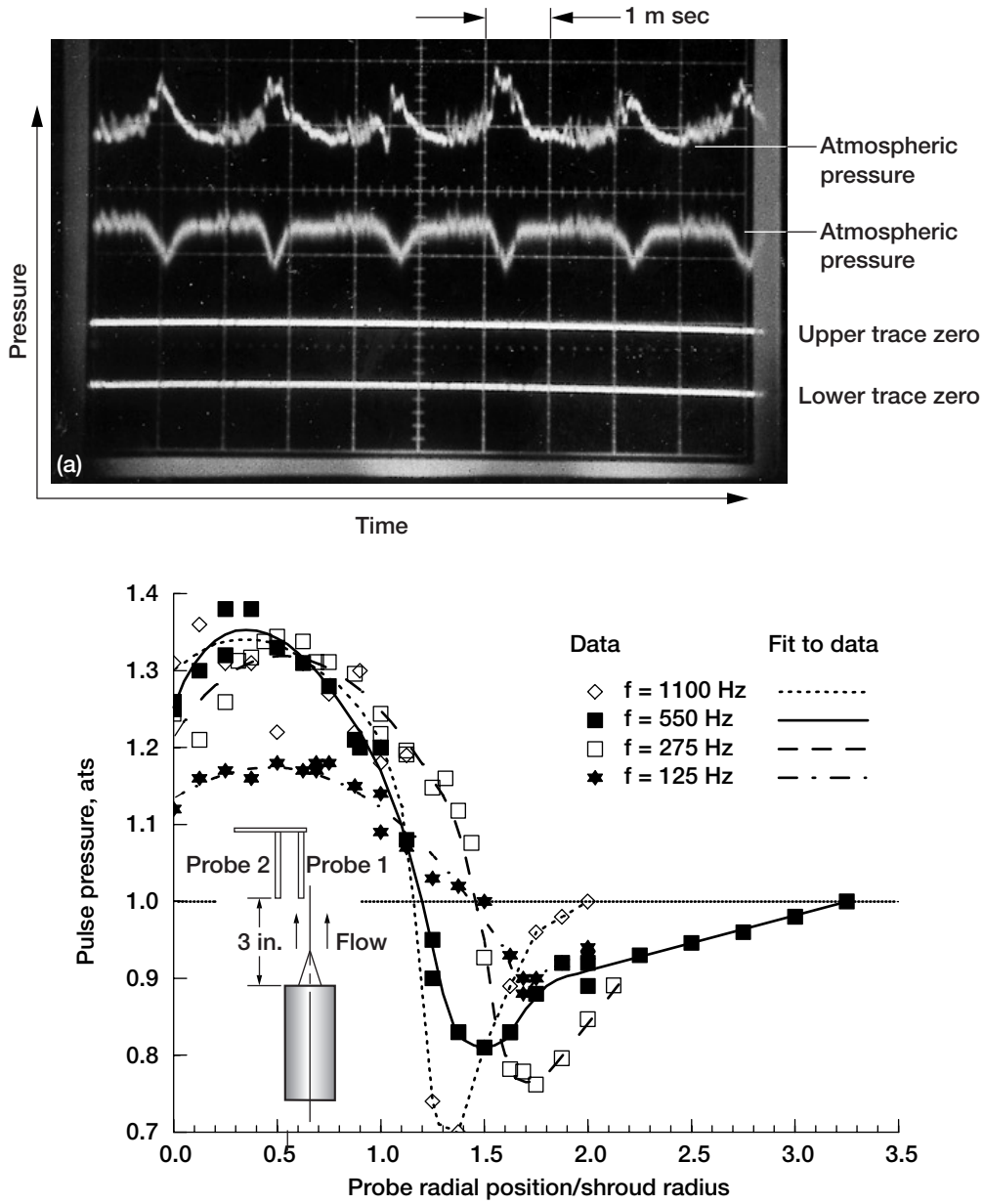

Figure 11.—(a) Oscillograms of high frequency pressure probe data. (b) Plot of the pressure pulse extrema versus normalized probe position for 1100 Hz, 550 Hz, 275 Hz, and 125 Hz, and fits to the data.

Table 3.—Measured vortex ring velocity, and thrust corrected vortex ring velocity

	f = 1100 Hz	f = 550 Hz	f = 275 Hz	f = 125 Hz
W from pitot probes (m/s)	73	77	83	77
W from LPIV			79	
Thrust (Newtons)	40	44.7	39.3	33.8
W corrected to 39.4 Newtons	72	68	83/79	89

Laser particle image velocimetry was used to measure velocities within the vortex ring, for a frequency of 275 Hz only. The values of axial velocity along a radius at the centre of the ring are plotted in figure 13. The velocity of the vortex ring itself is 79 m/s. This velocity occurs at the vortex radius R. The maxima and minima of velocity are at radii of $R - a$, and $R + a$ respectively, from which R = 33.3 mm, a = 18 mm, and hence $\varepsilon = 0.54$. A sketch of the vortex ring is on the right hand side of figure 12. The minimum signal from the pressure probes is at a radius of 43.2 mm, at which radius the velocity is zero. This radius is close to $R + a/2$. For greater radii, the velocity over the probes is negative, so they are not then acting as total pressure probes.

The LPIV data provide a map of vorticity ω over the entire field of view. The circulation in the vortex ring can be determined from this by performing the integral

$$K_{ring} = \iint \omega \, dr \, dz \tag{30}$$

The result is K_{ring} = 13.7 m^2/s. The integration was performed numerically from large radius to zero. The circulation increased as the radius decreased, reaching a maximum of 23.9 m^2s^{-1} at a radius of 15.8 mm, then decreasing to the value of 13.7 m^2s^{-1} on the centerline. This is a consequence of the flow coming from an annulus, so that vorticity shed from the inner diameter is of opposite sign from that generated at the outer diameter, thereby reducing the total circulation.

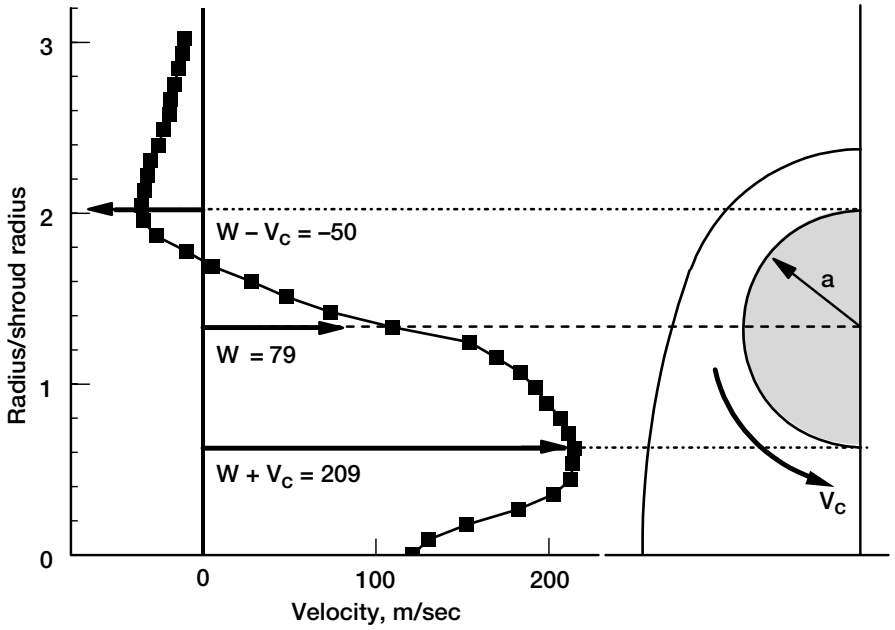

Figure 12.—Velocities on the r axis through the vortex ring as a function of normalized radial position. The velocities come from LPIV data. $V_c = K/2\pi a$ = 130 m/s is the velocity at the edge of the core.

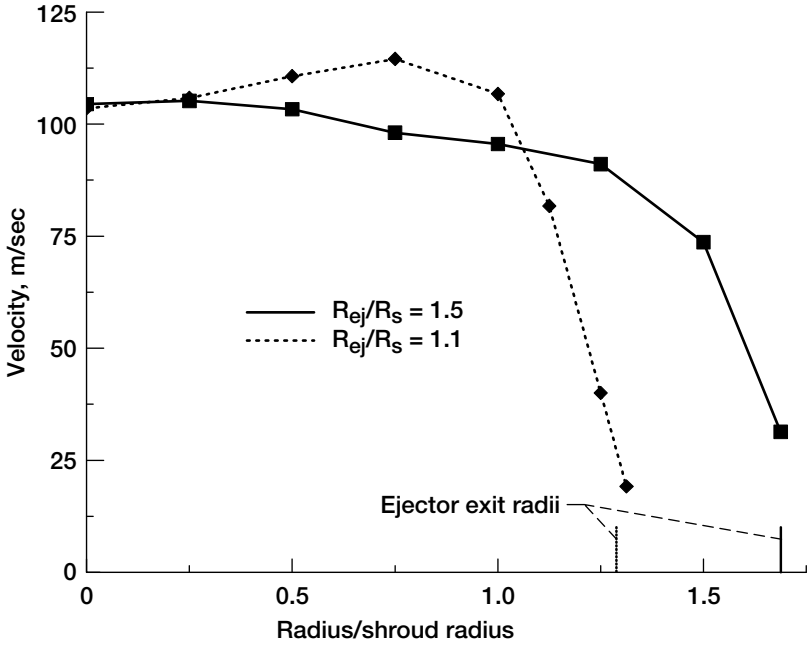

Figure 13.—Time averaged velocity at the ejector exit as a function of normalized radius. The data is from hot-wire measurements.

Ejector Exit Velocity

Measurements of ejector exit velocity were made using the 550 Hz source only, with the 27.9 mm radius and 38 mm radius ejectors. Initial attempts to use the high frequency pressure probes to sample the exit velocity of the ejector were abandoned as the signal was too small to be accurate. Instead, a hot wire was used to measure velocity. The signals showed periodic fluctuations in velocity, with the period equal to that of the source. The fluctuations were quite large; for example, with the hot-wire on the centerline of the 38 mm radius ejector, the average velocity was 93 m/sec, the maximum was 142 m/sec, and the minimum was 79 m/sec. The hot-wire was set at different radial positions, and the velocity measured. The resulting average velocity as a function of radius is shown in figure 13, for both ejectors. The distribution with radius is remarkably smooth, and the curves can be integrated to give the volume flow rate, and hence the mass entrainment factor β, defined as ingested mass divided by the jet mass flow. The resulting values of β are given in table 1. Dividing the volume flow rate by the area inside the ejector, πR_{ej}^2, gives an average velocity inside the ejector, which was 108 m/sec for the 38 mm radius ejector, 132 m/sec for the 28 mm radius ejector, i.e. larger than the vortex ring velocity.

Jet Exit Velocity

By placing one of the high frequency pressure probes used to sample the vortex ring exactly in the exit plane of the jet, a signal is obtained which can be related to the jet exit velocity. This was done at a frequency of 275 Hz only. The resulting velocity is plotted in figure 14. The flow starts with a weak shock wave (Mach number = 1.25), and, after an initial spike, is approximately constant for a while before falling off. An average flow exit velocity can be derived from the thrust, namely

$$U = T_{jet} / \dot{m}_{jet} \tag{31}$$

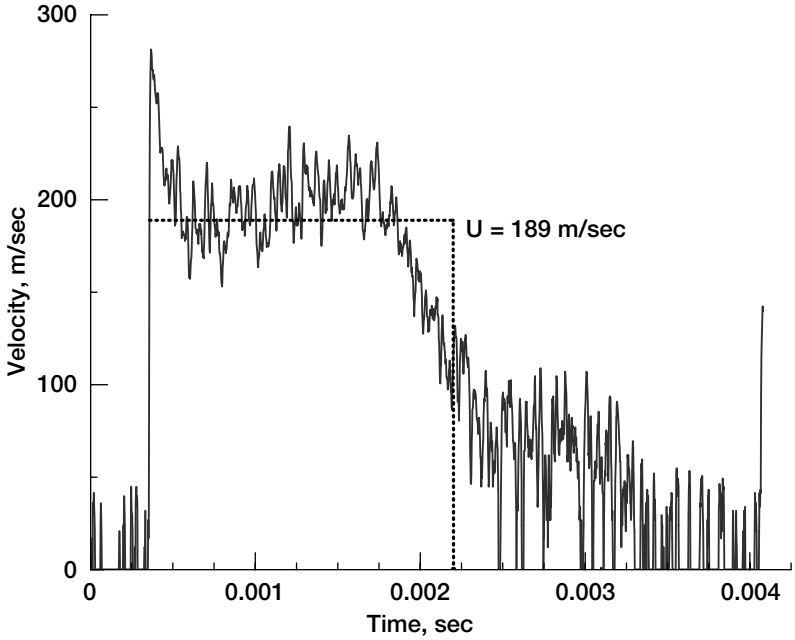

Figure 14.—Flow velocity at the exit of the Hartmann-Sprenger tube as a function of time, for f = 275 Hz. Data from the high frequency pressure probe.

This gives a value of 189 m/sec, which is also shown in figure 14, and is in good agreement with the probe results. The probe velocities can be integrated to give a value for $(U_2/U_1)^2$ of 1.1, the value used in figure 2(b) in deriving L/D versus α for a jet with velocity that is not constant with time.

Comparison Between the Slug Model and Experimental Results

The experiments were performed at four different frequencies. Since the mass flow was constant at all frequencies, the mass per pulse m_p is given by

$$m_p = \dot{m}_{jet} / f \tag{32}$$

in which f is frequency. But m_p is also given by the product of pulse volume and density

$$m_p = \rho \pi (D_s^2 - d_t^2) L/4 \tag{33}$$

from which it is seen that L/D is inversely proportional to frequency. In referring to the slug flow model, it is clear that the appropriate diameter appearing in L/D is twice the square root of the flow area divided by π, i.e. for the Hartmann–Sprenger tube it is $D = \sqrt{\left(D_s^2 - d_t^2\right)}$. In table 4 the values of L/D for each frequency used are given together with values of ε from (6b) for the two higher frequencies. For the lower frequencies, since the vortex probing showed that the vortex rings were the same size for both frequencies, ε is the same for both, and equal to the value measured from the LPIV data, namely 0.54. Gharib (1998) showed that above some cut-off value of L/D, the circulation of the vortex ring remains constant as L/D increases, with the remaining circulation going into a trailing jet. In Gharib's case, the limiting value of L/D was 4. If this were the case for the present experiments, the vortex rings for 550,

Table 4.—L/D and ε for each frequency used, together with the maximum thrust augmentation observed for each R_{ej}, as corrected to a thrust of 39.4 Newtons.

Frequency (Hz)	1100	550	275	125
L/D	2.5	5	10	22
ε	0.177	0.386	0.54	0.54
α_{max} for $R_{ej}/R_s = 1.1$	1.16	1.141	--	--
α_{max} for $R_{ej}/R_s = 1.5$	1.167	1.284	1.342	1.269
α_{max} for $R_{ej}/R_s = 2.0$	1.167	1.239	1.376	1.36
α_{max} for $R_{ej}/R_s = 3.0$	--	1.124	1.197	1.187

275, and 125 Hz, which all have L/D greater than 4, should all be the same size. In fact the 550 Hz vortex rings are smaller than those at 275 and 125 Hz. This indicates that the cut-off point appears at a higher value of L/D than 4. From (6b), the maximum value of ε observed, i.e. 0.54, occurs at an L/D of 6.86. This will then be taken to be the cut-off value, L/D_{co}, for these vortex rings.

The measurements at 275 and 125 Hz are at values of L/D above the cut-off point. In these cases the flow consists of a leading vortex ring and a trailing jet. The thrust on the ejector will be partially due to the vortex ring and partially to the trailing jet. There will be a time, t', following initiation of the jet at which the value of $L = \int_o^{t'} u(t)\mathrm{d}t$ corresponds to L/D_{co}. The fraction of the total jet impulse that is in this portion of the jet is

$$f_{vr} = \int_o^{t'} u(t)^2 \, \mathrm{d}t / \int_o^{\tau} u(t)^2 \, \mathrm{d}t \tag{34}$$

in which $\tau = 1/f$ is the period of the oscillations. It is this fraction of the impulse that goes into forming the vortex ring, giving rise to a thrust augmentation α_{vr}. The remaining impulse will be in the trailing jet, which will be assumed to create a thrust augmentation as would a steady jet. Thrust augmentation for a steady jet depends on the ratio of ejector area to jet area. In order to quantify this, the following expression was used for the steady thrust augmentation

$$\alpha_s = 1.0855 + 0.1043 \ln (D_{ej}^2/D^2) \tag{35}$$

This is consistent with a plot of α_s versus area ratio from Porter and Squyers (1979). Thus, for L/D greater than the cut-off value, the total thrust augmentation will be

$$\alpha_{total} = f_{vr} \, \alpha_{vr} + (1 - f_{vr}) \, \alpha_s \tag{36}$$

in which α_{vr} is calculated at cut-off. The value of f_{vr} was derived from the jet velocity distribution of figure 14. However, for computational purposes, it was more convenient to have an analytical expression, which was derived from assuming the velocity distribution is triangular, i.e. $u(t) = 2U\,(1 - t/\tau)$. It then follows that

$$t'/\tau = 1 - \sqrt{\left(1 - L/D_{co} \,/\, L/D\right)} \tag{37}$$

and

$$f_{vr} = 3\,(t'/\tau)\,(1 - t'/\tau + (t'/\tau)^2/3) \tag{38}$$

Results with the triangular model were in good agreement with the numerical results for the actual velocity distribution.

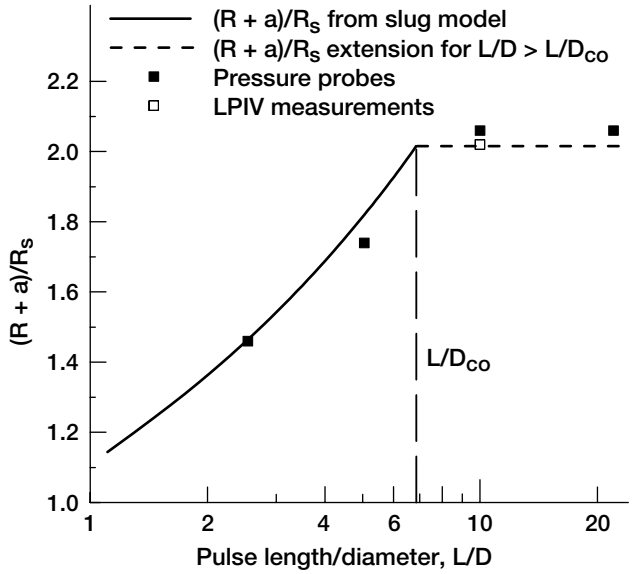

Figure 15.—Normalized value of (R + a) versus L/D.

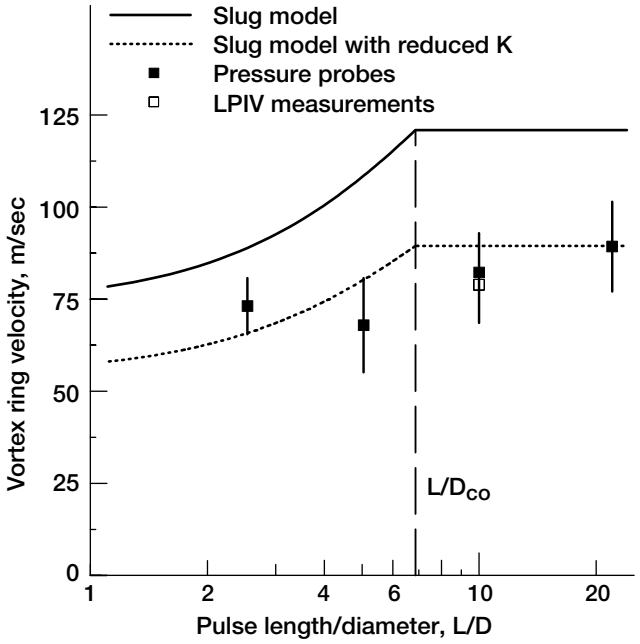

Figure 16.—Vortex ring velocity plotted against L/D as calculated from the slug model, vortex ring velocity with the slug model circulation multiplied by 0.72, and data from pressure probes and from LPIV measurements.

The probe measurements in figure 11(b) show that the pulse minima are at a value of r/R_s = 1.7 for the 275 and 125 Hz rings. The LPIV data in figure 12 indicate that this is the radius at which the velocity is zero, and is approximately equal to $R + a/2$. Assuming then that the probe minima are at a radius of $R + a/2$, and using the values of ε in table 4, the value of $R + a$ can be calculated for each frequency, and plotted against L/D. The results are shown in figure 15, together with the LPIV value at 275 Hz, and the calculated values from the slug model, assuming a cut-off at L/D = 6.86. The agreement is very good.

In figure 16, the observed vortex ring velocities, as corrected for thrust, are also plotted against L/D, together with the values calculated from the slug model, again assuming a cut-off at L/D = 6.86. The calculated values are too high, and better agreement with the measurements is obtained by multiplying the value of K_{ring} calculated from (3) in the slug model by 0.72. Doing so gives a calculated circulation of 14.4 m^2/s and vortex ring velocity of 80 m/s at ε = 0.54. This compares well with the value of K_{ring} = 13.7 m^2/s from the LPIV data and vortex ring velocities of 83 m/s from the probe measurements, and 79 m/s from the LPIV data. It might be thought that the high value of W calculated from the slug is because the value of Γ used in (3) is too high. However, Γ also appears in (8), the equation for the vortex ring radius, so if Γ were reduced, the good agreement between calculated and observed ring radius would be diminished. In fact the discrepancy is because the circulation calculated in (3) is based on the circulation created at the outer edge of the shroud only. As shown by the LPIV data, there is vorticity of opposite sign shed at the inner tube, which reduces the total circulation. Multiplying the calculated K_{ring} by 0.72 accounts for this, giving a value of K_{ring} in agreement with the measured value, as well as agreement between measured and calculated vortex ring velocity.

Using the factor 0.72 to correct K_{ring}, (20) can be used to calculate the thrust augmentation for L/D less than L/D_{co}, and (35) for L/D greater than L/D_{co}. The results in figure 17 show thrust augmentation plotted against ejector radius for both calculated and experimental thrust augmentation, corrected to a jet thrust of 39.4 Newtons. From (20) it can be seen that $(\alpha_{vr} - 1) \sim V_{ej}^2/T_{jet}$. The ejector velocity V_{ej} is assumed proportional to W, which scales with U, which in turn is proportional to T_{jet} since $\dot{m}_{jet}$ is

constant. Therefore $(\alpha_{vr} - 1) \sim T_{jet}$, and for comparison of the values of thrust augmentation at different frequencies, and hence different thrusts, the observed values of $(\alpha - 1)$ should be corrected by multiplying by $39.4/T_{jet}$. The corrected values of the maximum thrust augmentation observed at any one frequency and ejector radius, are listed in table 4, and plotted in figures 17 and 18. To fit the calculation to the data it was found that in (26) a value of $n = 1.5$ was optimum, and also that $R_{vr} = R + 2a/3$. Thus the optimum ejector diameter is $R + 2a/3$. The factor k was set equal to 1.37. This is not inconsistent with the value observed in the hot wire measurements. On the whole, the agreement between data and calculation is reasonable. In figure 18, the calculated and corrected experimental thrust augmentations are plotted against L/D, for a nose radius r_n/R_s of 0.5. Below L/D_{co}, the measured α is compared with (20), i.e. α_{vr}. Above L/D_{co}, the measured α is compared with (36), the calculated α_{total}. Again the agreement is reasonable. In particular, it is apparent that the calculation has the same trend as the data as regards the optimum ejector diameter; at low L/D, the 28 mm radius ejector is best, switching over to the 38 mm radius for an L/D of about 1.8 to 6, after which the 51 mm radius is best. In addition, for L/D greater than L/D_{co}, the calculations predict that as L/D increases, the thrust augmentation decreases for the ejectors with a radius of 51 mm or less, and increases for the ejector with a radius of 76 mm. The data exhibits the same trend. The steady state values of thrust augmentation are drawn in figure 18 as the horizontal lines on the right hand side. Above L/D_{co}, the data are heading towards these values.

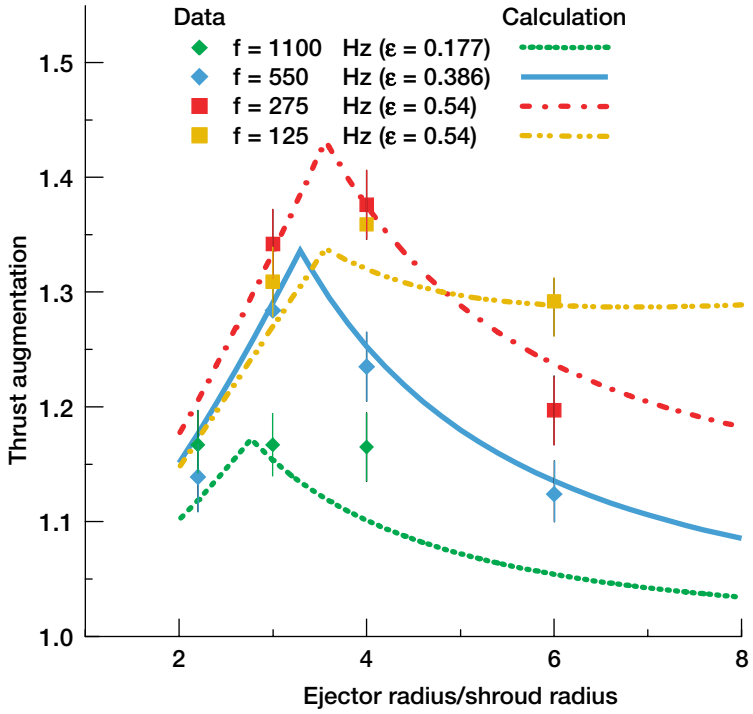

Figure 17.—Thrust augmentation versus normalized ejector radius. The calculations are from equation (20) for f = 1100 Hz and 550 Hz, and from equation (35) for f = 275 Hz and 125 Hz.

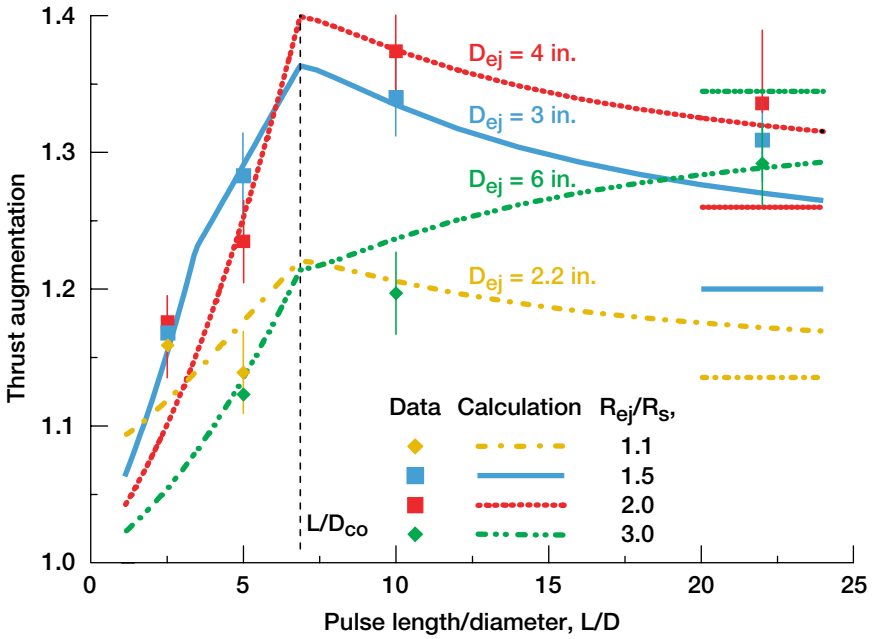

Figure 18.—Thrust augmentation plotted against L/D. The short horizontal lines at the right indicate the steady state thrust augmentation, i.e. thrust augmentation at L/D = ∞, for each ejector radius. The calculations are from equation (20) for $L/D < L/D_{co}$, from equation (35) for $L/D > L/D_{co}$.

Comments

The most controversial assumptions in this work are that the ejector flow is quasi-steady, and that the pressure at the trailing edge of the ejector is ambient. It is true that the observations of velocity at the exit of the ejector did exhibit significant oscillations, but the average flow velocity observed was in line with the value used in the calculation of thrust augmentation. The flow velocity at the ejector exit fell off with radius, and was small at the ejector lip, where the pressure was measured to be atmospheric. Had there been a large flow around the trailing edge, it could have generated suction, i.e. low pressure, and hence drag on the ejector. Since neither high flow velocity, nor low pressure was observed, there appears to be no significant drag on the trailing edge. Thus the assumptions do seem reasonable. Moreover, the resulting calculations seem to fit the data quite well.

What this model does not do is explain any effect of ejector length, yet the experiments clearly show that there is one, and that there is an optimum length. The longer the ejector is, the more frictional drag there will be, so a maximum length could be determined when friction is included. As constituted, the model can not explain why a short length is worse than the optimum length. Possibly this is because the entrained flow does not become a directed flow in a short length, but this is only speculation, and this point needs further study. These experiments indicate that a length of about twice the ejector diameter is optimum. This is longer than claimed by Lockwood (1961), but shorter than optimum length to diameter ratios found by Paxson et al. (2002), or Binder and Didelle (1975).

The calculations, when fitted to the experiments, do show an optimum ejector radius of $R_{ej} = R + 2a/3$. Since the larger the value of R_{ej} is, the greater the thrust augmentation will be, it behooves having the largest possible vortex ring radius R. The value of $R + 2a/3$ grows as L/D increases, up to L/D_{co}, but remains at this size for larger L/D. Thus the driving jet should be operated at L/D_{co}. At values of L/D greater than L/D_{co}, not only does $R + 2a/3$ remain fixed, but a smaller fraction of the total circulation goes to the vortex ring, and so the vortex ring thrust augmentation decreases. For very large values of L/D, higher thrust augmentation is possible at larger diameters, as indicated by the data for the

76 mm radius ejector at $L/D = 22$, but the augmentation will then correspond to the steady value. For steady ejectors, as stated above, high thrust augmentation is achieved with high ratios of R_{ej}/R_s, and the optimum L_{ej} appears to be around 2 to 4 times R_{ej}, so the ejector will be long.

Given that the optimum operating point for the driving jet is at L/D_{co}, an estimate can be made for the maximum possible thrust augmentation. At L/D_{co}, the value of $R + 2a/3$ is approximately equal to D. For a duty cycle of 0.5, appropriate for the Hartmann-Sprenger tube, the jet thrust is given by $0.5\ \rho U^2\ \pi D^2/4$. Inserting these relations, plus $V_{ej} = k\ W$, into (20) gives

$$\alpha_{vr} = 1 + \pi\ \rho\ (kW)^2\ F(\sigma)/\rho U^2\ \pi/8$$

$$= 1 + 8\ (kW/U)^2\ F(\sigma) \tag{39}$$

From the slug model, for a circular, i.e. non-annular exit, $W/U \approx 0.5$ at L/D_{co}, so with $k = 1.37$, and a reasonable value of $F(\sigma) = 0.3$, the maximum α_{vr} is 2.1. For the annulus used in these experiments, since W/U is less than 0.5, the maximum value of α_{vr} is 1.58.

Conclusions

In conclusion, the slug model appears to predict the vortex ring size and velocity correctly, provided proper account is taken of the dependence of circulation on L/D and exit geometry. The simple model of ejector performance, assuming a constant ejector velocity proportional to the vortex ring velocity, and dependant on ejector radius, does seem to explain some of the features of pulsed ejector flow, and predicts an optimum ejector radius of $R + 2a/3$. The optimum jet L/D for pulsed thrust augmentation is shown to be the cut-off value L/D_{co}. The maximum possible thrust augmentation possible is estimated to be about 2. For the annular exit used in the present experiment, since W/U is lower than for a circular exit, the maximum thrust is limited to 1.6.

References

Bertin, J. (1955) "Dilution pulsatoire sur réacteur," Comptes Rendues des Séances de l'Académie des Sciences, Vol. 240, pp. 1855–1857.

Binder, G. and Didelle, H. (1975) "Improvement of Ejector Thrust Augmentation by Pulsating or Flapping Jets," Paper E3 of Proc. 2nd Symposium on Jet Pumps & Ejectors and Gas Lift Techniques, Cambridge, England.

Brasseur, J.G. (1979) "Kinematics and Dynamics of Vortex Rings in a Tube," JIAA TR-26, Joint Institute for Aeronautics and Acoustics, Stanford University.

Brocher, E. (1975) "Contribution à l'étude des générateurs acoustique à jet d'air," Acustica, Vol. 32, pp. 227–235.

Brocher, E. and Pinna, G. (1980) "Aeroacoustical Phenomena in a Horn Excited by a Hartmann-Sprenger Tube," Acustica, Vol. 45, No. 3, pp. 180–189.

Das, D., Arakeri, J.H., Krothapalli, A., and Lourenco, L.M. (2001) "Compressible Vortex Ring: A PIV Study," Paper AIAA 2001–2214, presented at the 7th AIAA/CEAS Aeroacoustics Conference, Maastrich, Netherlands.

Didden, N. (1979) "On the formation of vortex rings: Rolling-up and production of circulation," J. Appl. Mech. Phys. (ZAMP) 30: 101–116.

Elder, F.K. and de Haas, N. (1952) "Experimental Study of the Formation of a Vortex Ring at the Open End of a Cylindrical Shock Tube," Journal of Applied Physics, 23, pp. 1065–1069.

Fraenkel, L.E. (1972) "Examples of steady vortex rings of small cross-section in an ideal fluid," J. Fluid Mech., 51, pp. 119–135.

Gharib, M., Rambod, E., and Shariff, K. (1998) "A universal time scale for vortex ring formation," J. Fluid Mech., 360, pp. 121–140.

Gradshteyn, I.S. and Ryzhik, I.M. (1994) "Table of Integrals, Series, and Products," Alan Jeffrey, Editor, Academic Press, New York.

Han, S. (2002) "Effects of the Primary Flow Pulse Frequency on the Secondary Flow Entrainment Rate," AIAA Paper 2002–2857.

John, W.T., Paxson, D.E., and Wernet, M.P. (2002) "Conditionally Sampled Pulsejet Driven Ejector Flow Field Using DPIV," AIAA Paper 2002–3231.

Johnson, W.S. and Yang, T. (1968) "A Mathematical Model for the Prediction of the Induced Flow in a Pulsejet Ejector with Experimental Verification," ASME Paper 68–WA/FE–33.

Krutsch, C-H. (1939) "Ueber eine experimentell beobachte Erscheinung an Wirbelringen bei ihrer translatorischen Bewegung in wirklichen Fluessigkeiten," Annalen der Physik, 5, Folge, Band 53, pp. 497–523.

Lamb, Sir H. (1932) "Hydrodynamics," Dover, New York.

Liess, C., and Didden, N. (1975) "Experimentelle Untersuchung von Ringwirbeln," 50 Jahre M.P.I. Stroemungsforschung, Goettingen.

Linden, P.F., and Turner, J.S. (2001) "The formation of 'optimal' vortex rings, and the efficiency of propulsion devices," J. Fluid Mech., 427, pp. 61–72.

Lockwood, R.M. (1961) "Interim Summary Report on Investigation of the Process of Energy Transfer from an Intermittent Jet to Secondary Fluid in an Ejector-type Thrust Augmenter," Hiller Aircraft Report No. ARD–286.

Marzouk, E-S.M., and Wahab, A.F.A. (1997) "A Numerical Model for Prediction of the Induced Flow in Pulse Ejector with Experimental Verification," AIAA Paper 97–1016.

Mason, R.L., Gunst, R.F., and Hess, J.L. (1989) "Statistical Design and Analysis of Experiments: with Applications to Engineering and Science," Wiley, New York.

Maxworthy, T. (1977) "Some experimental studies of vortex rings," J. Fluid Mech. 81: 465–495.

Norbury, J. (1973) "A family of steady vortex rings," J. Fluid Mech., 57, pp. 417–431.

Paxson, D.E., Wilson, J., and Dougherty, K.T. (2002) "Unsteady Ejector Performance: An Experimental Investigation using a Pulsejet Driver," Paper AIAA–2002–3915, presented at the 38th Joint AIAA/ASME/SAE/ASEE Propulsion Conference, Indianapolis, IN.

Porter, J.L., and Squyers, R.A. (1979) "A Summary/Overview of Ejector Augmentor Theory and Performance, Phase II – Technical Report," Vought Corporation Advanced Technology Center Report No. R–91100/9CR–47A.

Seshadri, S. and Demming, S.N. "Box-B Interactive Computer Programs for using Three- and Four-Factor Box-Behnken Designs in Research, Development, and Manufacturing (version 2.1)," This program is available from: Statistical Programs, 9941 Rowlett, Suite 6, Houston, TX 77075.

Shariff, K., and Leonard, A. 1992 "Vortex Rings," Ann. Rev. Fluid Mech., 24, pp. 235–279.

Wilson, J., and Paxson, D.E. (2002) "Unsteady Ejector Performance: An Experimental Investigation using a Resonance Tube Driver," Paper AIAA–2002–3632, presented at the 38th Joint AIAA/ASME/SAE/ASEE Propulsion Conference, Indianapolis, IN.

REPORT DOCUMENTATION PAGE

Form Approved
OMB No. 0704-0188

1. AGENCY USE ONLY (*Leave blank*)	2. REPORT DATE	3. REPORT TYPE AND DATES COVERED
	August 2003	Final Contractor Report

4. TITLE AND SUBTITLE

A Simple Model of Pulsed Ejector Thrust Augmentation

5. FUNDING NUMBERS

WBS–22–708–48–01
NAS3–00145

6. AUTHOR(S)

Jack Wilson

7. PERFORMING ORGANIZATION NAME(S) AND ADDRESS(ES)

QSS Group, Inc.
21000 Brookpark Road
Cleveland, Ohio 44135

8. PERFORMING ORGANIZATION REPORT NUMBER

E–14107

9. SPONSORING/MONITORING AGENCY NAME(S) AND ADDRESS(ES)

National Aeronautics and Space Administration
Washington, DC 20546–0001

10. SPONSORING/MONITORING AGENCY REPORT NUMBER

NASA CR—2003-212541

11. SUPPLEMENTARY NOTES

Project Manager, Richard L. Deloof, Aeronautics Directorate, NASA Glenn Research Center, organization code 2400, 216–433–6632.

12a. DISTRIBUTION/AVAILABILITY STATEMENT

Unclassified - Unlimited
Subject Category: 02 Distribution: Nonstandard

Available electronically at http://gltrs.grc.nasa.gov

This publication is available from the NASA Center for AeroSpace Information, 301–621–0390.

12b. DISTRIBUTION CODE

13. ABSTRACT ***(Maximum 200 words)***

A simple model of thrust augmentation from a pulsed source is described. In the model it is assumed that the flow into the ejector is quasi-steady, and can be calculated using potential flow techniques. The velocity of the flow is related to the speed of the starting vortex ring formed by the jet. The vortex ring properties are obtained from the slug model, knowing the jet diameter, speed, and slug length. The model, when combined with experimental results, predicts an optimum ejector radius for thrust augmentation. Data on pulsed ejector performance for comparison with the model was obtained using a shrouded Hartmann-Sprenger tube as the pulsed jet source. A statistical experiment, in which ejector length, diameter, and nose radius were independent parameters, was performed at four different frequencies. These frequencies corresponded to four different slug length to diameter ratios, two below cut-off, and two above. Comparison of the model with the experimental data showed reasonable agreement. Maximum pulsed thrust augmentation is shown to occur for a pulsed source with slug length to diameter ratio equal to the cut-off value.

14. SUBJECT TERMS

Ejectors; Thrust augmentation; Hartmann-Sprenger tubes

15. NUMBER OF PAGES

31

16. PRICE CODE

17. SECURITY CLASSIFICATION OF REPORT	18. SECURITY CLASSIFICATION OF THIS PAGE	19. SECURITY CLASSIFICATION OF ABSTRACT	20. LIMITATION OF ABSTRACT
Unclassified	Unclassified	Unclassified	